

Your Room is not Private: Gradient Inversion Attack on Reinforcement Learning

Miao Li¹, Wenhao Ding¹, Ding Zhao¹

Abstract—The prominence of embodied Artificial Intelligence (AI), which empowers robots to navigate, perceive, and engage within virtual environments, has attracted significant attention, owing to the remarkable advancements in computer vision and large language models. Privacy emerges as a pivotal concern within the realm of embodied AI, as the robot accesses substantial personal information. However, the issue of privacy leakage in embodied AI tasks, particularly in relation to reinforcement learning algorithms, has not received adequate consideration in research. This paper aims to address this gap by proposing an attack on the value-based algorithm and the gradient-based algorithm, utilizing gradient inversion to reconstruct states, actions, and supervision signals. The choice of using gradients for the attack is motivated by the fact that commonly employed federated learning techniques solely utilize gradients computed based on private user data to optimize models, without storing or transmitting the data to public servers. Nevertheless, these gradients contain sufficient information to potentially expose private data. To validate our approach, we conduct experiments on the AI2THOR simulator and evaluate our algorithm on active perception, a prevalent task in embodied AI. The experimental results demonstrate the effectiveness of our method in successfully reconstructing all information from the data across 120 room layouts.

I. INTRODUCTION

The advent of recent large foundation models has brought about remarkable achievements in human-like dialog generation [1] and controllable image generation [2]. These achievements highlight the promising potential of leveraging artificial intelligence (AI) to enhance human experiences. The next significant milestone in the advancement of general AI revolves around the exploration of embodied systems, such as household robots, that possess the ability to navigate, perceive, engage, and successfully tackle tasks within the physical world.

The process of collecting embodied datasets presents more privacy concerns in comparison to language and vision tasks, as the robot operates within real-world environments, executing policies, and gathering observational signals. These environments often contain personal information [3], [4], which presents challenges during data collection and model training. To address the need to preserve sensitive information, the *Federated Learning* framework [5] is introduced. This framework allows local storage of private data on individual machines, with only the gradients, calculated based on the private information within the environment [6]–[9], being transmitted to the central server. These gradients, originating from multiple private servers, are then aggregated

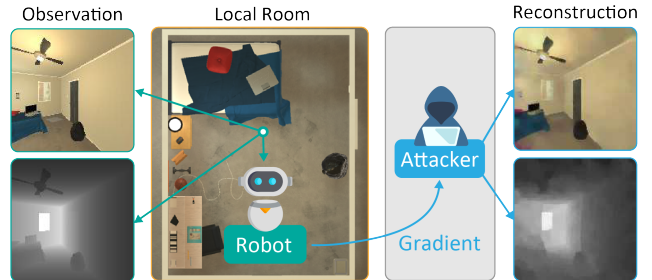


Fig. 1: Our method (Attacker) can reconstruct the images of your untidy room and window orientation from the gradient.

and utilized to update the policy model on the central server. Subsequently, the updated model is sent back to the private servers for the next optimization iteration. As a result, the model and gradients are accessible publicly, while the data remains accessible only to private servers.

However, relying solely on the transmission of gradients still leaves room for vulnerability to gradient inversion techniques [10]–[13], a type of method that can reconstruct input images and labels from the corresponding gradients in classification tasks. The gradient inversion algorithms either search for realistic synthetic images in latent spaces using generative networks [14] or directly optimize a synthetic image in the image domain, initialized by heuristic methods. The accuracy of the reconstruction is optimized by a loss function that compares the real gradient sent by the private server with the gradient produced using the synthetic data. Concurrently, the visual quality of the reconstructed image is ensured through loss functions based on prior knowledge, such as the smoothness of natural images [10]–[12], [15]. These techniques can reconstruct high-resolution images with recognizable patterns using gradients from mini-batches with small batch sizes [11], [16]. Although not all reconstructed images are necessarily recognizable, these studies highlight the privacy risks, namely the leakage of private training data, associated with federated learning.

Motivated by the existing literature on gradient inversion in classification tasks, our research aims to address the privacy leakage issue in reinforcement learning (RL) within the context of embodied AI, an area that has received limited attention thus far. Fig. 1 provides an illustrative example of this problem, demonstrating how an attacker can successfully reconstruct RGB and depth images of a room solely from the gradient. Unlike in classification tasks where the input typically consists of a single RGB image, applying gradient inversion techniques to RL poses unique challenges due to the multimodal nature of the input information including

¹Carnegie Mellon University, Pittsburgh, PA 15213, USA. Email: {limiao, wenhaod, dingzhao}@andrew.cmu.edu

image state, vector state, action, and reward. Our objective is to reconstruct all these inputs exclusively from the gradients shared by the RL algorithm. The most relevant work to this topic is [17], which reconstructs the location map from the model parameter of Deep Q Network (DQN) [18]. However, this approach is limited in that it supports only one map for one model, and it focuses on a trained model other than the learning process.

In this work, we introduce a novel gradient inversion approach targeting the value-based RL algorithm and the gradient-based RL algorithm, namely *Deep Q-learning Gradient Inversion (QGI)* and *REINFORCE Gradient Inversion (RGI)*. We address the task of multimodal data reconstruction from the gradient of RL algorithms. Specifically, we initialize the reconstructed state with Gaussian noises and optimize it with cosine similarity between the gradients of the true and reconstructed data. An additional prior term is used to penalize noisy image patterns. Unlike in classification tasks where the input is only RGB images, gradient inversion in reinforcement learning is challenging due to the multimodal input. We propose a pipeline for multimodal input and rule-based methods for action and supervision signal reconstruction. We follow the white-box assumption [19] and honest-but-curious assumption [11] of the potential adversary, which does not modify the model or the optimization process. We evaluate QGI and RGI in the AI2THOR [20] simulator on the active perception task [21]–[23], a popular task in embodied AI to navigate agents to obtain higher detection accuracy of the given object. Our main contributions are summarized:

- As far as we know, QGI and RGI are the first frameworks to investigate the information leaking problem by reconstructing data in RL from the gradient.
- We provide novel pipelines to reconstruct multimodal information of states, actions, and supervision signals.
- We evaluate our method in a realistic simulation of the active perception task and show that our QGI and RGI can successfully reconstruct all information.

II. RELATED WORK

Privacy attack in Deep Learning. Private training data is at risk of attacks, including membership inference, model inversion, and gradient inversion [24]. Membership inference assumes the adversary has access to certain data and attempts to verify whether the data is used in the training procedure [25], [26], while in robotic tasks, the private environments tend to stay inaccessible to adversaries, for example, bedrooms of private property. In contrast, model inversion and gradient inversion assume the private data is inaccessible and the adversary attempts to reconstruct the data, which are of higher significance for robotic tasks. While model inversion reveals the training data from the trained model [19], [27]–[29], gradient inversion tackles the reconstruction from the gradients shared in federated, collaborative, decentralized, or distributed learning [10]–[12], [14], [16], [30].

Gradient inversion. Previous works in gradient inversion mainly focused on image classification tasks. Zhu et al. first

formulated the gradient inversion technique and proposed an end-to-end optimization method DLG to reconstruct both images and labels for the classification task from single-sample gradients and batched gradients [10]. Zhao et al. [13] proposed an efficient method to identify the one-hot label from a single-sample gradient. Geiping et al. [11] extended gradient inversion to high-resolution images by minimizing a prior loss proven effective in image denoising [31] and model inversion [28] and a magnitude-agnostic cosine similarity loss function. We adopt this loss function in this work. Yin et al. [16] increased the accuracy under large batch sizes by leveraging prior loss functions and penalizing differences in results from multiple trials. While most works studied CNN or MLP, GradViT [12] attacked gradients of Vision Transformer by designing prior terms aiming at the architecture. Generative networks are introduced to achieve image reconstruction in the specific domain [14], [15]. Based on [10], Deng et al. [32] reconstructed data of Transformer-based language models. To the best of our knowledge, gradient inversion is unexplored in the realm of both robotic tasks and multi-modal data.

Privacy in Reinforcement Learning. Privacy has been studied in existing Reinforcement Learning literature for a long time. However, most works dedicated to privacy-preserving [3], [4], [33]–[35] other than revealing the risk of privacy leakage. The most relevant work for this paper in Reinforcement Learning is [17]. They reconstructed the training environment from the trained policies, demonstrating the privacy risk of releasing trained models. Based on the prior knowledge, they used the genetic algorithm to search for the configuration of the environment. While they studied the sensitive information contained in trained models, the risk associated with the training procedure remains ambiguous. In this work, we investigate the possibility of revealing private state, action, and Q-values from gradients, where the data can change through the training procedure and the number of data samples is unlimited.

III. PRELIMINARY

Gradient Inversion. Gradient inversion aims to reconstruct the training data from the gradient of the model, which can be employed by the potential adversary when the training data is invisible but the gradient is shared, for example, in federated learning. Given the input of the network x , the supervision signal u (e.g., label in classification), the model F with parameters w , the output $y = F(x; w)$, and the objective function J , then the gradient g is

$$g = \nabla_w J(F(x; w), u) = \frac{\partial J(y, u)}{\partial y} \frac{\partial F(x; w)}{\partial w}. \quad (1)$$

The gradient carries the information of x in the $\frac{\partial F(x; w)}{\partial w}$ and the information of u in the $\frac{\partial J(y, u)}{\partial y}$, which can be utilized by an honest-but-curious [11], [17] adversary. The goal of gradient inversion is to reconstruct (x, u) by generating $(x^{\text{rec}}, u^{\text{rec}})$ that produces gradient g^{rec} , which is sufficiently close to the true gradient g . Assuming the adversary has white-box access to the model F and the objective J , then the reconstructed

gradient is $g^{\text{rec}}(x^{\text{rec}}, u^{\text{rec}}) = \nabla_w J(F(x^{\text{rec}}; w), u^{\text{rec}})$. The adversary minimizes the gradient matching loss function $L(g^{\text{rec}}, g)$ to obtain reconstruction $x^{\text{rec}}, u^{\text{rec}}$ as follows

$$(x^{\text{rec}}, u^{\text{rec}}) = \arg \min_{\tilde{x}, \tilde{u}} L(\tilde{g}(\tilde{x}, \tilde{u}), g(x, u)). \quad (2)$$

Markov Decision Process, DQN and REINFORCE. We consider Markov Decision Process (MDP) as the mathematical framework to model decision-making problems in reinforcement learning. MDP consists of state space $s \in \mathcal{S}$, action space $a \in \mathcal{A}$, reward function $r \in \mathcal{R}$, and a transition model $p \in \mathcal{P}$. The future discounted return at timestep t is $R_t = \sum_{t'=t}^T \gamma^{t'-t} r_{t'}$, where γ is the discount factor and T is the maximal step. In this paper, we investigate the gradient inversion in the DQN algorithm [18], which estimates the optimal action-state value function (Q-value)

$$Q^*(s, a) = \max_{\pi} \mathbb{E}[R_t | s_t = s, a_t = a, \pi], \quad (3)$$

where π is a policy mapping sequences to actions. Empirically, this $Q^*(s, a)$ is parameterized with neural networks and the objective is minimizing the difference between the predicted Q-value $\hat{Q}(s, a)$ of the selected action a and the target Q-value $Q(s, a)$ with transitions (s_t, a_t, s_{t+1}, r_t) from the replay buffer. We also investigate gradient inversion attack for the REINFORCE algorithm [36] with the entropy term, which utilizes the policy gradient to update the policy. The gradient of the policy model is estimated as

$$\nabla_{\theta} J = \mathbb{E}[\log \pi_{\theta}(s) R_t] - \alpha \nabla_{\theta} \pi_{\theta}(s) \log \pi_{\theta}(s), \quad (4)$$

where J is the total objective function and α is the weight of entropy term.

Active Perception Task. Active Perception [21]–[23] is a prevalent embodied AI task that allows robots to capture data in a better position to increase the confidence and accuracy of detection. Since it requires private information about the user room, we select it as the example task to apply the gradient inversion attack. In this task, the state contains depth image s_d , RGB image s_i , and coordinate s_c that indicates the position of the target object in the images. The action space is discrete with seven movement options. Similarly to [21], the reward is defined by the confidence score obtained from an object detection model. The policy network predicts Q-values $\hat{Q}(s, a)$ for all possible actions given the input $s = \{s_d, s_i, s_c\}$. The images are first processed by convolution layers F_{conv} , while the coordinate vector is processed by linear layers. Their features are concatenated and processed by linear layers. F_{linear} demonstrates all the linear layers.

IV. METHOD

In this section, we introduce gradient inversion on reinforcement learning, a method to reconstruct one training data sample from the gradient of reinforcement learning algorithms, including the multimodal state s , action a , and supervision signal, for example, the target Q-value $Q(s, a)$ or reward r . Note that the reward may not be recoverable when not using the gradient calculation. We propose to reconstruct input data of different modal types in separate

optimization steps to solve (2), which outperforms the joint optimization. The objective functions in reinforcement learning algorithms may cause challenges during reconstructed gradient calculation. Therefore, we propose to calculate the reconstructed gradient g^{rec} from the error direction, instead of the original objective function, which allows us to use rule-based methods to reconstruct the action and supervision signal. Despite we focus on single-sample gradients, the attack on batched gradients can also benefit from the insight.

We illustrate the details of the proposed method through the implementation of the gradient inversion attack on two reinforcement learning algorithms, DQN [18] and REINFORCE [36]. We show the entire pipeline for Gradient Inversion on DQN (QGI) and REINFORCE (RGI) in Fig. 2. QGI contains the following steps. In **step 1**, action is identified by a rule-based method. In **step 2**, we reconstruct the multimodal state by optimization in two stages. Stage 1 targets the input of all linear layers, including the coordinate vector s_c . Stage 2 reconstructs the image states, including RGB s_i and depth s_d images. In **step 3**, we estimate the predicted Q-value $\hat{Q}^{\text{rec}}(s, a)$ by feeding the reconstructed vectors, and the target Q-value Q^{rec} by a rule-based method. RGI also contains 3 steps. In **step 1**, we reconstruct the probability for each possible action by optimization. In **step 2**, we reconstruct the action and reward by a rule-based method. In **step 3**, the multimodal state is reconstructed in two stages the same as in QGI.

A. Optimization-Based Multimodal State Reconstruction

As shown in Fig. 2, we separate the state reconstruction into 2 stages for both QGI and RGI. In each stage, we initialize the reconstruction of the corresponding state with Gaussian noise and use gradient descent to optimize the reconstruction. We first reconstruct the vector state and then reconstruct the image state with the vector state fixed.

Our victim task has two image states, namely the RGB image s_i and depth image s_d , and one vector state, namely the coordinate s_c indicating a target object bounding box. Specifically, we initialize the coordinate and image reconstruction with Gaussian noises. We optimize the vector state with the gradient matching loss $L(g^{\text{rec}}, g)$. In addition to the gradient matching loss, we further add a prior term for the image state. We adopt the cosine similarity loss from [11],

$$L(g^{\text{rec}}, g) = 1 - \frac{\langle g^{\text{rec}}, g \rangle}{\|g^{\text{rec}}\|_2 \|g\|_2}. \quad (5)$$

The total variation (TV) loss [31] is added with weight λ for image state reconstruction to penalize noisy patterns, leading to the total loss $L_{\text{img}} = L(g^{\text{rec}}, g) + \lambda(\text{TV}(s_i) + \text{TV}(s_d))$.

B. Error-Direction-Based Gradient Calculation

Optimization-based gradient inversion minimizes the gradient matching loss for the reconstructed gradient g^{rec} as shown in (2), where g^{rec} is usually calculated by back-propagation after feeding the reconstructed training data, i.e. $g^{\text{rec}} = \nabla_w J(F(x^{\text{rec}}; w), u^{\text{rec}})$. As objective functions in reinforcement learning may contain special calculations and

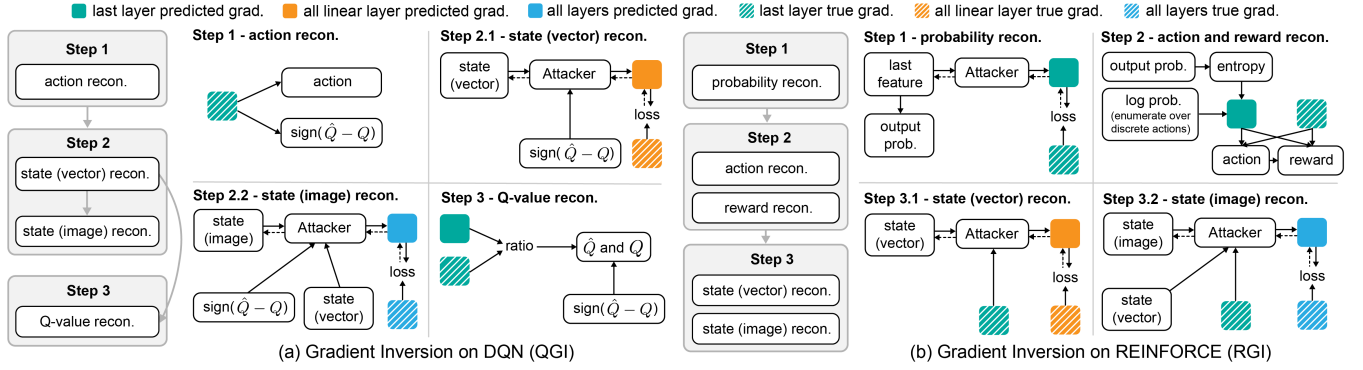


Fig. 2: Pipeline of the proposed gradient inversion attack on DQN (left) and REINFORCE (right). The left part of each image shows the steps to reconstruct the multimodal information, and the right part explains each step in detail.

data flow that compromise the performance, we propose to interpret the gradient as the result of backpropagation from an error direction $\frac{\partial J}{\partial y}$ other than from objective function J . When the batch size is 1 and the last layer of the network is a linear layer with a bias parameter, this error direction is equal to the gradient of the last layer's bias parameter $\nabla_{b_{\text{last}}} J(F(x), u)$. Thus, we propose a surrogate objective

$$\tilde{J}(F(x^{\text{rec}}), u^{\text{rec}}) = (\nabla_{b_{\text{last}}} J(F(x), u))^{\top} F(x^{\text{rec}}), \quad (6)$$

and use \tilde{J} for the g^{rec} calculation. The gradient from \tilde{J} is the same as from J when the reconstructed data $(x^{\text{rec}}, u^{\text{rec}})$ are the same as (x, u) . Therefore, the optimal solution for (2) is still the true training data.

C. Rule-based Reconstruction for QGI

1) *Action Reconstruction:* Since the action space of DQN is discrete, we propose to directly identify the action from the gradient when the batch size is only 1 or 2. Observe that the predicted Q-value $\hat{Q}(s, \cdot)$ is obtained from the last linear layer with weight W_{last} and bias b_{last} , and the objective $J(\hat{Q}(s, a), Q(s, a))$ only provides one non-zero value for $\hat{Q}(s, a)$, where the action a is taken by the policy. Then we can obtain the action from the gradient of the bias $\nabla_{b_{\text{last}}}$

$$\nabla_{b_{\text{last}}} = \frac{\partial J(\hat{Q}(s, a), Q(s, a))}{\partial \hat{Q}(s, a)} \underbrace{\frac{\partial \hat{Q}(s, a)}{\partial \hat{Q}(s)}}_{\text{one-hot vector}} \underbrace{\frac{\partial \hat{Q}(s)}{\partial b_{\text{last}}}}_{\mathbf{1}}. \quad (7)$$

When $\frac{\partial J(\hat{Q}, Q)}{\partial \hat{Q}} \neq 0$, only the a -th element of b_{last} has a non-zero gradient, which allows us to identify the action. When the batch size is larger than 2, the action reconstruction may require enumeration or optimization.

2) *Q-value Reconstruction:* The reconstruction of target Q-values Q is implemented in 3 stages, (1) reconstructing the sign of the error $\tilde{n} = \text{sign}(\hat{Q} - Q)$, (2) reconstructing the magnitude of the error $\hat{Q} - Q$, (3) reconstructing Q based on the the reconstructed error and the reconstructed \hat{Q}^{rec} , where \hat{Q}^{rec} is obtained by feeding the state reconstruction. The sign \tilde{n} can be identified from the gradient of the last linear layer, as shown in Fig. 2. The magnitude of the error is obtained from the ratio $\|g\|/\|g^{\text{rec}}\|$. Since the objective function is the mean square error (MSE), the gradient of parameter w is

$g = \frac{\partial J(\hat{Q}, Q)}{\partial \hat{Q}} \frac{\partial \hat{Q}}{\partial w} = 2(\hat{Q} - Q) \frac{\partial \hat{Q}}{\partial w}$. The relationship between the error and gradients is $\frac{\|\hat{Q} - Q\|}{\|\hat{Q}^{\text{rec}} - \hat{Q}\|} \frac{\partial \hat{Q} / \partial w}{\partial \hat{Q}^{\text{rec}} / \partial w} = \frac{\|g\|}{\|g^{\text{rec}}\|}$, where \hat{Q} is a constant used as the target Q-value during gradient inversion that produces the accurate error direction. Once the vector inputs are obtained in step 2.1, we feed the vector reconstruction to the network and obtain the reconstruction of the predicted Q-value \hat{Q}^{rec} . We assume the reconstructions of vector inputs are accurate. Then \hat{Q}^{rec} is accurate and $\frac{\partial \hat{Q} / \partial w}{\partial \hat{Q}^{\text{rec}} / \partial w} = 1$, and the magnitude of the error between the predicted and the target Q-value is reconstructed by $\|\hat{Q} - Q\|^{\text{rec}} \leftarrow \|\hat{Q}^{\text{rec}} - \hat{Q}\| \frac{\|g\|}{\|g^{\text{rec}}\|}$. The reconstruction of the target Q-value is then obtained as $Q^{\text{rec}} \leftarrow \hat{Q}^{\text{rec}} - \tilde{n} \|\hat{Q} - Q\|^{\text{rec}}$.

D. Rule-based Reconstruction for RGI

The action and reward of REINFORCE are reconstructed by rule-based methods in RGI, as shown in Fig. 2. After conducting optimization-based gradient inversion on the last linear layer and reconstructing the input feature of the last linear, we feed the reconstruction through the last layer and reconstruct the output, namely the probability of all actions p^{rec} . Note that the objective function for REINFORCE has two components, namely the policy gradient term J_{pg} and the entropy term J_{entropy} . While the J_{pg} calculation involves both action and reward, J_{entropy} only depends on the probability. Thus, we focus on the component from J_{pg} , reconstructed as

$$(\nabla_{b_{\text{last}}} J_{\text{pg}})^{\text{rec}} = \nabla_{b_{\text{last}}} - (\nabla_{b_{\text{last}}} J_{\text{entropy}}(p^{\text{rec}})), \quad (8)$$

to reconstruct the action and reward. Given the calculation in (4), the direction of this component depends on the action, while the magnitude depends on the reward. To decide the action, we propose to enumerate all possible actions and calculate the corresponding $\nabla_{b_{\text{last}}} J_{\text{pg}}(p^{\text{rec}}, a^{\text{rec}}, r^{\text{rec}})|_{r^{\text{rec}}=1}$ by feeding the $(p^{\text{rec}}, a^{\text{rec}}, r^{\text{rec}})$ through the normal gradient calculation process. We choose the action that leads to the direction of $(\nabla_{b_{\text{last}}} J_{\text{pg}})^{\text{rec}}$. The reward is reconstructed as

$$r^{\text{rec}} = \frac{(\nabla_{b_{\text{last}}} J_{\text{pg}})^{\text{rec}}}{\nabla_{b_{\text{last}}} J_{\text{pg}}(p^{\text{rec}}, a^{\text{rec}}, \hat{r})} \Big|_{\hat{r}=1}. \quad (9)$$

V. EXPERIMENT

Experimental setup. We conducted evaluations of our method on an active perception task using the AI2THOR

TABLE I: PSNR (\uparrow) and SSIM (\uparrow) of the RGB and depth images.

method	setting	State	Metric	bathroom	bedroom	kitchen	living room	average	best
QGI	S1	RGB	PSNR	22.81 \pm 5.99	19.73 \pm 5.16	21.41 \pm 5.69	20.11 \pm 6.17	21.02 \pm 5.86	32.17
			SSIM	0.761 \pm 0.141	0.735 \pm 0.146	0.724 \pm 0.167	0.696 \pm 0.170	0.729 \pm 0.157	0.929
		depth	PSNR	24.89 \pm 10.43	22.85 \pm 7.42	23.26 \pm 7.17	21.72 \pm 7.05	23.18 \pm 8.17	38.09
			SSIM	0.809 \pm 0.249	0.823 \pm 0.161	0.803 \pm 0.197	0.793 \pm 0.162	0.807 \pm 0.195	0.983
QGI	S2	depth	PSNR	29.78 \pm 7.33	26.14 \pm 7.67	26.45 \pm 7.27	23.49 \pm 7.29	26.46 \pm 7.68	45.76
			SSIM	0.930 \pm 0.111	0.899 \pm 0.152	0.918 \pm 0.092	0.894 \pm 0.129	0.910 \pm 0.123	0.994
RGI	S1	RGB	PSNR	18.03 \pm 5.76	16.98 \pm 5.93	17.65 \pm 4.85	15.84 \pm 4.60	17.12 \pm 5.35	31.20
			SSIM	0.564 \pm 0.190	0.550 \pm 0.186	0.551 \pm 0.166	0.511 \pm 0.163	0.544 \pm 0.176	0.924
		depth	PSNR	19.75 \pm 6.66	18.80 \pm 6.26	18.71 \pm 5.35	17.04 \pm 5.17	18.58 \pm 5.94	36.41
			SSIM	0.582 \pm 0.197	0.590 \pm 0.164	0.594 \pm 0.158	0.559 \pm 0.141	0.581 \pm 0.166	0.940
RGI	S2	depth	PSNR	39.19 \pm 5.34	37.87 \pm 3.57	36.91 \pm 4.31	34.85 \pm 4.99	37.21 \pm 4.84	58.83
			SSIM	0.972 \pm 0.018	0.968 \pm 0.018	0.963 \pm 0.022	0.953 \pm 0.024	0.964 \pm 0.022	1.000

simulator [20]. In the primary setting (S1), private observations were collected using an RGB and a depth camera, each with a resolution of 150×150 . Additionally, we explored the performance in a setting where only a depth camera was available (S2), aiming to examine the privacy risks associated with widely used depth images in robotic tasks. The target object’s bounding box was specified by the 4-dimensional coordinate from the upstream task within the range of $[-1, 1]$. Gradients were calculated for individual data samples fed into an initialized network. λ is 0.1. The optimization-based reconstruction involved 2×10^4 iterations. Quantitative evaluation was performed on 240 pre-collected samples. Results of real-world data can be found in the video.

Metric. To assess the quality and accuracy of the reconstructed state, action, predicted Q-value, target Q-value, and reward, we have selected several metrics for evaluation. For the image state, we utilize two metrics: **peak-signal-to-noise ratio (PSNR)** and **structure-similarity index measure (SSIM)** [37]. PSNR and SSIM are computed on the Y channel of the YCbCr representation for RGB images and the single channel for depth images. Based on prior knowledge of the AI2THOR environment, we normalize the reconstructed RGB images so that the brightest pixel has a value of 255 in the S1 setting, and the corresponding depth image is scaled by the same factor. For the coordinate state, which represents a bounding box, we calculate the **intersection over union (IoU)** metric to measure accuracy. The accuracy of the action is evaluated by simply counting the number of accurate results. We employ the **percentage error**, denoted as $\epsilon(x) = 100 \times \frac{|x^{rec} - x|}{|x|}$, to evaluate the predicted and target Q-values. We also test predicted Q-values, as errors of predicted Q-value and target Q-value are related. Lastly, we use absolute error to evaluate the reward.

A. Quantitative Results

State: RGB and Depth Image. Table I presents the PSNR and SSIM values for the images. In the S1 setting, where both RGB and depth images are available, the mean PSNR of the RGB images of QGI is over 21dB, and the mean SSIM is over 0.7, indicating the images are recognizable to humans, potentially leaking information about the layout of the environments and private elements to potential adversaries. The

depth images exhibit higher PSNR and SSIM, suggesting that the rooms’ size and the objects’ distance are at risk of privacy leakage. In the S2 setting, the adversary may find it more challenging due to the lack of color information. However, the reconstructed depth images are highly accurate. As shown in Table I, PSNR and SSIM increase by over 4dB for QGI and over 15dB for RGI across all room types, primarily due to the lower dimensionality of the input data.

State: Coordinate. The mean IoU of both QGI and RGI reaches over 0.9 for both settings. For QGI, 174 samples achieved IoU larger than 0.9999 in the S1 setting, while 217 samples achieved that in the S2 setting. For RGI, 238 samples achieved that in both 2 settings. Despite the large error of the failure cases, these results indicate that the adversary can reconstruct the vector state input data.

Predicted Q-value, Target Q-value, and Reward. The percentage errors of predicted and target Q-values are significantly small, with a mean of less than 1.1% and a standard derivative of less than 1.6% for both settings. The absolute error of the reward reconstruction in RGI has a mean value smaller than 1×10^{-6} for both 2 settings. These results indicate the attacker can reconstruct the supervision signal.

Action. The action identified from the gradient of a single sample is 100% correct in all 240 samples, which demonstrates the effectiveness of the rule-based method. The method used in QGI is generalizable for other RL algorithms with MSE loss functions, and the method in RGI is generalizable for other policy-gradient-based RL algorithms.

B. Qualitative Results

The qualitative results are shown in Fig. 3 for both QGI and RGI in 2 settings. Results of the S1 setting are shown in the left part. Both the RGB and depth images are reconstructed with recognizable patterns and magnitudes. The RGB images exhibit accurate color tones, despite some colored noise in local areas. The depth images display similar noisy patterns, but the overall brightness of continuous areas remains accurate. Consequently, the sizes of private rooms can be accessed by adversaries. In the S2 setting, as depicted in the right part, the reconstructed depth images exhibit accuracy with clear edges and details.



Fig. 3: Qualitative results. The left shows the results of depth+RGB images (S1). The right shows the results of depth images (S2). The upper shows the results of QGI. The lower shows the results of RGI.

TABLE II: Ablation study for error-direction-based method (Opt: joint optimization, Rule: rule-based, Cos: cosine similarity).

Method	Gradient Calculation	Action	Target Q	Loss	IoU (\uparrow)	$\epsilon(\hat{Q})(\%)$ (\downarrow)	$\epsilon(Q)(\%)$ (\downarrow)
based on DLG [10]	objective J	Opt	Opt	MSE	0.649 ± 0.401	1083.64 ± 6434.83	89.85 ± 12.28
based on DLG [10]	objective J	Rule	Opt	MSE	0.610 ± 0.408	1112.33 ± 6676.23	92.44 ± 8.42
based on inverting [11]	objective J	Rule	Opt	Cos	0.216 ± 0.342	15751.95 ± 93392.97	198.83 ± 292.31
QGI (ours)	error direction $\nabla_{b_{last}}$	Rule	Rule	Cos	0.912 ± 0.0192	1.03 ± 0.159	0.67 ± 0.147

C. Ablation Study

We evaluate the effect of the proposed separate optimization of the multimodal state by comparing it with the joint optimization of the image state (RGB+depth) and vector state (goal coordinate) in QGI. As shown in Fig. 4, the joint optimization shows performance drops for all metrics. Besides the lower mean value, PSNR and SSIM have larger standard derivatives, indicating an unstable reconstruction. The mean IoU is below 0.1, while QGI achieves over 0.9. Q-value reconstructions also show a performance decline.

We also evaluate the proposed error-direction-based gradient calculation by comparing it with the normal gradient calculation from the objective function. As the objective function requires the action and target Q-value as input, these data need to be either reconstructed before the optimization-based gradient inversion or jointly optimized. We optimize the target Q-value reconstruction jointly with input and test both rule-based and jointly optimized action reconstruction. As the magnitude of the gradient is essential for the target

Q-value reconstruction, we also introduce the MSE gradient matching loss. These designs resemble DLG [10] and inverting gradient [11]. DLG [10] jointly optimized the input and classification label with MSE loss, while inverting gradient [11] adopted the label identification from iDLG [13] and used cosine similarity loss to optimize the input. As shown in Table II, our method shows the best results, indicating better reconstruction for both input and supervision signal.

VI. CONCLUSION

This paper introduces a novel privacy leakage study on reinforcement learning algorithms, namely DQN and REINFORCE, as privacy leakage is a critical concern but has not received significant attention in the existing literature of reinforcement learning. Given the challenge of adapting existing gradient inversion algorithms to handle multi-modal inputs in RL, we develop a comprehensive pipeline that iteratively reconstructs the inputs. Through experimental results in active perception tasks, we demonstrate that QGI and RGI successfully reconstruct the image state, vector state, action, and supervision signal from the gradient. Ablation studies further validate the advantage of our proposed design.

One limitation of this work is that the batch size is constrained to a small number to maintain the quality of the reconstruction. As pioneers in this area, we recognize the importance of addressing the privacy leakage problem to build a trustworthy embodied AI system. Therefore, we leave the exploration of larger batch sizes and extensions to other RL-based decision-making algorithms for future research.

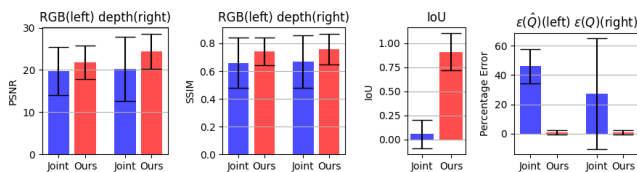


Fig. 4: Ablation study of multimodal state reconstruction. Comparison of joint optimization (joint) and our method.

REFERENCES

- [1] L. Ouyang, J. Wu, X. Jiang, D. Almeida, C. Wainwright, P. Mishkin, C. Zhang, S. Agarwal, K. Slama, A. Ray, *et al.*, “Training language models to follow instructions with human feedback,” *Advances in Neural Information Processing Systems*, vol. 35, pp. 27730–27744, 2022.
- [2] A. Ramesh, P. Dhariwal, A. Nichol, C. Chu, and M. Chen, “Hierarchical text-conditional image generation with clip latents,” *arXiv preprint arXiv:2204.06125*, 2022.
- [3] J. Sakuma, S. Kobayashi, and R. N. Wright, “Privacy-preserving reinforcement learning,” in *Proceedings of the 25th international conference on Machine learning*, 2008, pp. 864–871.
- [4] B. Wang and N. Hegde, “Privacy-preserving q-learning with functional noise in continuous spaces,” *Advances in Neural Information Processing Systems*, vol. 32, 2019.
- [5] C. Zhang, Y. Xie, H. Bai, B. Yu, W. Li, and Y. Gao, “A survey on federated learning,” *Knowledge-Based Systems*, vol. 216, p. 106775, 2021.
- [6] B. McMahan, E. Moore, D. Ramage, S. Hampson, and B. A. y Arcas, “Communication-efficient learning of deep networks from decentralized data,” in *Artificial intelligence and statistics*. PMLR, 2017, pp. 1273–1282.
- [7] J. Konečný, B. McMahan, and D. Ramage, “Federated optimization: Distributed optimization beyond the datacenter,” *arXiv preprint arXiv:1511.03575*, 2015.
- [8] J. Konečný, H. B. McMahan, D. Ramage, and P. Richtárik, “Federated optimization: Distributed machine learning for on-device intelligence,” *arXiv preprint arXiv:1610.02527*, 2016.
- [9] S. Reddi, Z. Charles, M. Zaheer, Z. Garrett, K. Rush, J. Konečný, S. Kumar, and H. B. McMahan, “Adaptive federated optimization,” *arXiv preprint arXiv:2003.00295*, 2020.
- [10] L. Zhu, Z. Liu, and S. Han, “Deep leakage from gradients,” *Advances in neural information processing systems*, vol. 32, 2019.
- [11] J. Geiping, H. Bauermeister, H. Dröge, and M. Moeller, “Inverting gradients-how easy is it to break privacy in federated learning?” *Advances in Neural Information Processing Systems*, vol. 33, pp. 16937–16947, 2020.
- [12] A. Hatamizadeh, H. Yin, H. R. Roth, W. Li, J. Kautz, D. Xu, and P. Molchanov, “Gradvit: Gradient inversion of vision transformers,” in *Proceedings of the IEEE/CVF Conference on Computer Vision and Pattern Recognition*, 2022, pp. 10021–10030.
- [13] B. Zhao, K. R. Mopuri, and H. Bilen, “idlg: Improved deep leakage from gradients,” *arXiv preprint arXiv:2001.02610*, 2020.
- [14] J. Jeon, K. Lee, S. Oh, J. Ok, *et al.*, “Gradient inversion with generative image prior,” *Advances in neural information processing systems*, vol. 34, pp. 29898–29908, 2021.
- [15] Z. Wang, M. Song, Z. Zhang, Y. Song, Q. Wang, and H. Qi, “Beyond inferring class representatives: User-level privacy leakage from federated learning,” in *IEEE INFOCOM 2019-IEEE conference on computer communications*. IEEE, 2019, pp. 2512–2520.
- [16] H. Yin, A. Mallya, A. Vahdat, J. M. Alvarez, J. Kautz, and P. Molchanov, “See through gradients: Image batch recovery via grad-inversion,” in *Proceedings of the IEEE/CVF Conference on Computer Vision and Pattern Recognition*, 2021, pp. 16337–16346.
- [17] X. Pan, W. Wang, X. Zhang, B. Li, J. Yi, and D. Song, “How you act tells a lot: Privacy-leaking attack on deep reinforcement learning,” in *AAMAS*, 2019, pp. 368–376.
- [18] V. Mnih, K. Kavukcuoglu, D. Silver, A. A. Rusu, J. Veness, M. G. Bellemare, A. Graves, M. Riedmiller, A. K. Fidjeland, G. Ostrovski, *et al.*, “Human-level control through deep reinforcement learning,” *nature*, vol. 518, no. 7540, pp. 529–533, 2015.
- [19] B. Hitaj, G. Ateniese, and F. Perez-Cruz, “Deep models under the gan: information leakage from collaborative deep learning,” in *Proceedings of the 2017 ACM SIGSAC conference on computer and communications security*, 2017, pp. 603–618.
- [20] E. Kolve, R. Mottaghi, W. Han, E. VanderBilt, L. Weihs, A. Herrasti, M. Deitke, K. Ehsani, D. Gordon, Y. Zhu, *et al.*, “Ai2-thor: An interactive 3d environment for visual ai,” *arXiv preprint arXiv:1712.05474*, 2017.
- [21] W. Ding, N. Majcherczyk, M. Deshpande, X. Qi, D. Zhao, R. Madhivanan, and A. Sen, “Learning to view: Decision transformers for active object detection,” *arXiv preprint arXiv:2301.09544*, 2023.
- [22] K. Kotar and R. Mottaghi, “Interactron: Embodied adaptive object detection,” in *Proceedings of the IEEE/CVF Conference on Computer Vision and Pattern Recognition*, 2022, pp. 14860–14869.
- [23] P. Ammirato, P. Poirson, E. Park, J. Košecká, and A. C. Berg, “A dataset for developing and benchmarking active vision,” in *2017 IEEE International Conference on Robotics and Automation (ICRA)*. IEEE, 2017, pp. 1378–1385.
- [24] M. Rigaki and S. Garcia, “A survey of privacy attacks in machine learning,” *arXiv preprint arXiv:2007.07646*, 2020.
- [25] R. Shokri, M. Stronati, C. Song, and V. Shmatikov, “Membership inference attacks against machine learning models,” in *2017 IEEE symposium on security and privacy (SP)*. IEEE, 2017, pp. 3–18.
- [26] N. Carlini, F. Tramer, E. Wallace, M. Jagielski, A. Herbert-Voss, K. Lee, A. Roberts, T. B. Brown, D. Song, U. Erlingsson, *et al.*, “Extracting training data from large language models,” in *USENIX Security Symposium*, vol. 6, 2021.
- [27] S. An, G. Tao, Q. Xu, Y. Liu, G. Shen, Y. Yao, J. Xu, and X. Zhang, “Mirror: Model inversion for deep learning network with high fidelity,” in *Proceedings of the 29th Network and Distributed System Security Symposium*, 2022.
- [28] A. Mordvintsev, C. Olah, and M. Tyka, “Inceptionism: Going deeper into neural networks,” 2015.
- [29] H. Yin, P. Molchanov, J. M. Alvarez, Z. Li, A. Mallya, D. Hoiem, N. K. Jha, and J. Kautz, “Dreaming to distill: Data-free knowledge transfer via deepinversion,” in *Proceedings of the IEEE/CVF Conference on Computer Vision and Pattern Recognition*, 2020, pp. 8715–8724.
- [30] X. Jin, P.-Y. Chen, C.-Y. Hsu, C.-M. Yu, and T. Chen, “Cafe: Catastrophic data leakage in vertical federated learning,” *Advances in Neural Information Processing Systems*, vol. 34, pp. 994–1006, 2021.
- [31] L. I. Rudin, S. Osher, and E. Fatemi, “Nonlinear total variation based noise removal algorithms,” *Physica D: nonlinear phenomena*, vol. 60, no. 1-4, pp. 259–268, 1992.
- [32] J. Deng, Y. Wang, J. Li, C. Shang, H. Liu, S. Rajasekaran, and C. Ding, “Tag: Gradient attack on transformer-based language models,” *arXiv preprint arXiv:2103.06819*, 2021.
- [33] G. Vietri, B. Balle, A. Krishnamurthy, and S. Wu, “Private reinforcement learning with pac and regret guarantees,” in *International Conference on Machine Learning*. PMLR, 2020, pp. 9754–9764.
- [34] E. Garcelon, V. Perchet, C. Pike-Burke, and M. Pirota, “Local differential privacy for regret minimization in reinforcement learning,” *Advances in Neural Information Processing Systems*, vol. 34, pp. 10561–10573, 2021.
- [35] M. Taherisadr, S. A. Stavroulakis, and S. Elmalaki, “adaparl: Adaptive privacy-aware reinforcement learning for sequential-decision making human-in-the-loop systems,” *arXiv preprint arXiv:2303.04257*, 2023.
- [36] R. J. Williams, “Simple statistical gradient-following algorithms for connectionist reinforcement learning,” *Machine learning*, vol. 8, pp. 229–256, 1992.
- [37] Z. Wang, A. C. Bovik, H. R. Sheikh, and E. P. Simoncelli, “Image quality assessment: from error visibility to structural similarity,” *IEEE transactions on image processing*, vol. 13, no. 4, pp. 600–612, 2004.